Click Here
for
Full
Article

Effects of vegetation and soil moisture on the simulated land surface processes from the coupled WRF/Noah model

Seungbum Hong,[1] Venkat Lakshmi,[1] Eric E. Small,[2] Fei Chen,[3] Mukul Tewari,[3] and Kevin W. Manning[3]

[1]   The coupled Weather Research and Forecasting (WRF) model with the Noah land surface model (Noah LSM) is an attempt of the modeling community to embody the complex interrelationship between land surface and atmosphere into numerical weather or climate prediction. This study describes coupled WRF/Noah model tests to evaluate the model sensitivity and improvement through vegetation fraction (Fg) parameterizations and soil moisture initialization. We utilized the 500 m 8-day Moderate Resolution Imaging Spectroradiometer reflectance data to derive the model Fg parameter using two different methods: the linear and quadric methods. In addition, combining the Fg quadric method, we initialized soil moisture simulated by High-Resolution Land Data Assimilation System, which has been developed for providing better soil moisture data in high spatial resolution by National Center for Atmospheric Research. We performed temporal comparisons of the simulated land surface variables: surface temperature (TS), sensible heat flux (SH), ground heat flux (GH), and latent heat flux (LH) to observed data during 2002 International H_2O Project. Then these results were statistically validated with correlation coefficients and root mean square errors. The results indicate high sensitivity of the coupled model to vegetation fluctuations, showing overestimation of vegetation transpiration and very low variability of GH in highly vegetated area.

Citation: Hong, S., V. Lakshmi, E. E. Small, F. Chen, M. Tewari, and K. W. Manning (2009), Effects of vegetation and soil moisture on the simulated land surface processes from the coupled WRF/Noah model, *J. Geophys. Res.*, *114*, D18118, doi:10.1029/2008JD011249.

1.   Introduction

[2]   Various atmospheric and land surface models have been developed to understand the complex hydrological cycle and provide improved forecasting simulations. Mesoscale models, which have been used not only for numerical weather prediction but also regional climate simulations, have been rapidly developed with increasing spatial and temporal resolutions [*Chen et al.*, 1997; *Pielke et al.*, 1997]. Numerical weather prediction with high spatial and temporal resolution provides valuable information for meteorological and agricultural applications on a regional scale [e.g., *Venäläinen et al.*, 2006]. Moreover, as the importance of interactions between land and atmosphere has been increasingly recognized, there have been attempts at model coupling techniques between land surface models and mesoscale models to complement local mesoscale water vapor circulations by land surface forcing [e.g., *Chen and Dudhia*, 2001; *Zeng et al.*, 2002]. The coupling techniques with atmospheric and land surface models are expected to provide deeper insight into the complex interrelationships between the atmosphere and land surface than what is seen in the uncoupled mode.

[3]   In this study, we selected the coupled Noah Land Surface model (Noah LSM)/Weather Research and Forecasting model (WRF). Furthermore, this study started from the technical issues of the model, which are defined as (1) Overestimation of latent heat (LH) flux most likely induced by vegetation effects (S. Hong et al., Interactions between the land surface and the atmosphere: Results from the Noah LSM and the WRF model, submitted to *Journal of Hydrometeorology*, 2009) and (2) absence of routine soil moisture observations on a regional and global scale for the model's initial condition. In a previous study (Hong et al., submitted manuscript, 2009), even though proper soil moisture initialization from field observation data for several locations resulted in reasonable simulations of soil moisture variations, LH simulations responded very sensitively to those variations, showing overestimations when soil moisture and vegetation were relatively high. In the Noah LSM, the green vegetation fraction, Fg, which is defined as the coverage of vegetation over a defined area such as a pixel, plays a very important role in the determination of the each component of evapotranspiration (ET). However, the Fg parameter used in the current LSM came from 5 years worth of monthly Advanced Very High Resolution Radiom-

---

[1]Department of Geological Sciences, University of South Carolina, Columbia, South Carolina, USA.
[2]Department of Geological Sciences, University of Colorado at Boulder, Boulder, Colorado, USA.
[3]National Center for Atmospheric Research, Boulder, Colorado, USA.

eter (AVHRR) data (1986–1991) with 0.15° of spatial resolution, which is about 15 km in Central America [*Gutman and Ignatov*, 1998]. Considering that one of the merits of the recently advanced WRF model is to provide simulations with very high resolution of 1 km or higher, the Fg parameter in the coarser resolution may negatively affect model accuracy and reliability for finer scale simulations. In terms of temporal resolution, monthly Fg data cannot provide enough information to describe short-term variations of land cover such as weekly or biweekly periods [*Hong et al.*, 2007]. Anthropogenic activities such as crop harvest may cause a large change in land cover over a period of a few weeks. An interannually invariant Fg parameter is also not congruous to annual land cover changes. Such limits on the Fg application tend to be overestimated, leading to an overestimation of the LH [*Montandon and Small*, 2008]. Thus, Fg is required to be parameterized with more compatible temporal and spatial resolution for improved model simulations.

[4] The absence of routine soil moisture measurements on a regional scale leads to a low model dependency on soil moisture variation and its effects. Current model systems are mostly assimilated with other modeling outputs such as the National Center for Environmental Prediction (NCEP) final analysis data with a resolution of 1 degree and 6 h and the NCEP regional operational Eta with a resolution of 40 km and 6 h. More recently, technical development of land surface and atmospheric observation has been contributing to data quality improvement, but still model data have been used as the base. For example, NASA and NOAA are providing North American Land Data Assimilation System (NLDAS) which has been recently improved from Eta/EDAS model data with various observations for higher resolution (1/8 degree and hourly). All available soil moisture data are not compatible with finer model simulations, e.g., that with the 1 km resolution that is used in this study. Coarse resolutions of initial data are generally followed by more interpolations to produce finer resolution outputs in the model. The differences in these spatial resolutions cause model biases.

[5] From the issues mentioned above, this paper provides model tests to evaluate simulation improvements of the WRF/Noah model through vegetation parameterization and soil moisture data initialization on a regional scale using remote sensing data and a land data assimilation system. First, in order to test model improvement and reliability on Fg parameterization with better vegetation observation data, we applied two different Fg derivation methods to the model parameterization. The two derivation methods utilized satellite derived Normalized Difference Vegetation Indices (NDVI) from Moderate Resolution Imaging Spectroradiometer (MODIS) surface reflectances. Recent remote sensing observation technology has made it possible to monitor atmospheric and land surface processes temporally and spatially in high resolution. For example, MODIS provides daily data with up to a 250 m resolution. Thus, with the help of the remotely monitored land surface data, we expect to complement the model weaknesses in terms of temporal and spatial resolution. Additionally, for more reliable model tests for Fg parameterization, we applied the measured soil moisture data to the model input by

replacing several soil moisture pixel values whose geographic locations correspond to measurement stations in our study area. We tested soil moisture data produced by the High-Resolution Land Data Assimilation System (HRLDAS), which was developed by NCAR [*Chen et al.*, 2007], and utilized these data as the model's initial condition. Combined with one of the Fg parameterization methods, the HRLDAS soil moisture initialization was performed to examine its effect on the sensitivity of the coupled model. Then, the results of the test are evaluated and it can be demonstrated that the HRDLAS soil moisture complements the lack of routine soil moisture observation data in the model.

[6] Simulation outputs from the model were compared to field observation data collected during the International H₂O project in 2002 (IHOP_2002) and the results were interpreted to evaluate how sensitive the model simulations are to temporal and spatial variations of land surface associated with vegetation distribution and soil moisture changes. The results of these model sensitivity experiments in the model coupled system will provide a direction for improved forecasting associated with surface moisture status.

2. Data and Methods

2.1. Study Areas and Observation Data

[7] The main goal of IHOP_2002 was to obtain accurate and reliable measurements of the near surface moisture status, which is very important for parameterization of a weather forecasting model [*Weckwerth et al.*, 2004]. These observations with various ground measurement devices were carried out during the growing season from May to June 2002. This study provided a contribution to forecasting skill improvement, better understanding and prediction of convective rainfall, improved understanding of the relationship between atmospheric water vapor and land surface processes, and future water vapor measurement strategies. During the IHOP_2002 period, NCAR installed nine surface flux stations, called Integrated Surface Flux Facilities (ISFF), to support the IHOP_2002 atmospheric boundary mission in the Southern Great Plains of the United States [*LeMone et al.*, 2007]. The flux stations were located in between Eastern Kansas and the Oklahoma Panhandle and were categorized as western (sites 1, 2, and 3), central (sites 4, 5, and 6), and eastern (sites 7, 8, and 9) tracks as seen in Figure 1. The stations along the western track are located from south to north in the Oklahoma panhandle, and the ones along the central and eastern track are aligned west to east southwest of Wichita, Kansas. The area around each station track demonstrates a characteristic surface condition related to soil moisture and vegetation cover. Along the western track, MODIS NDVI was in between 0.1 and 0.4, and soil moisture at a depth of 5 cm was less than 0.1 m³ m⁻³ in a dry period from 20 May to 27 May 2002. On the other hand, the eastern area including the eastern ISFF stations had relatively high soil moisture with over 0.3 m³ m⁻³ on average and high NDVIs in between 0.5 and 0.9. The eastern area has more vegetation and lower surface temperature than the western area [*LeMone et al.*, 2007]. The NCAR ISFF stations provide a suite of meteorological,
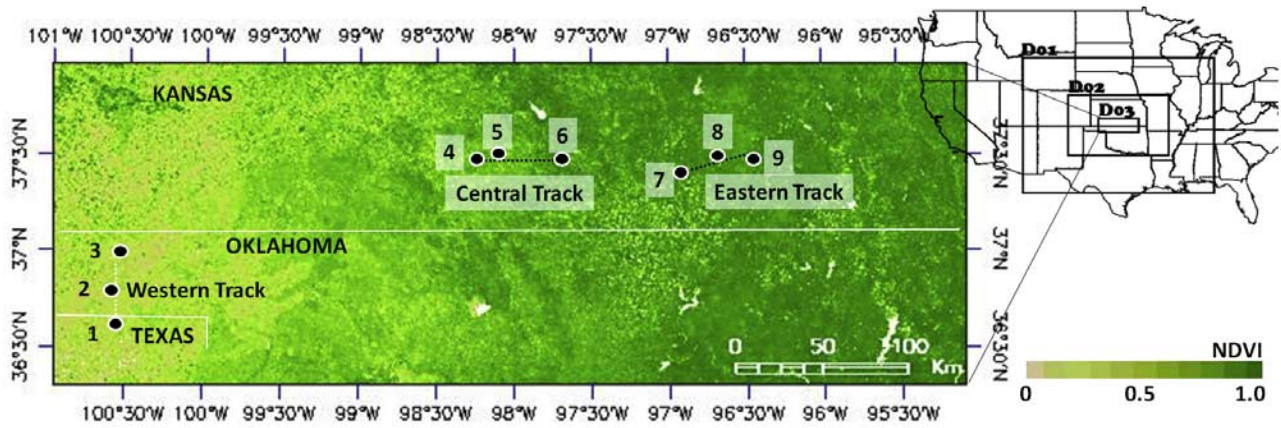
Figure 1. Image of the study area with MODIS NDVI distribution over the IHOP_2002 study region and the model domain configuration scheme; dots with denoted numbers in the image indicate the locations of the nine ISFF stations.
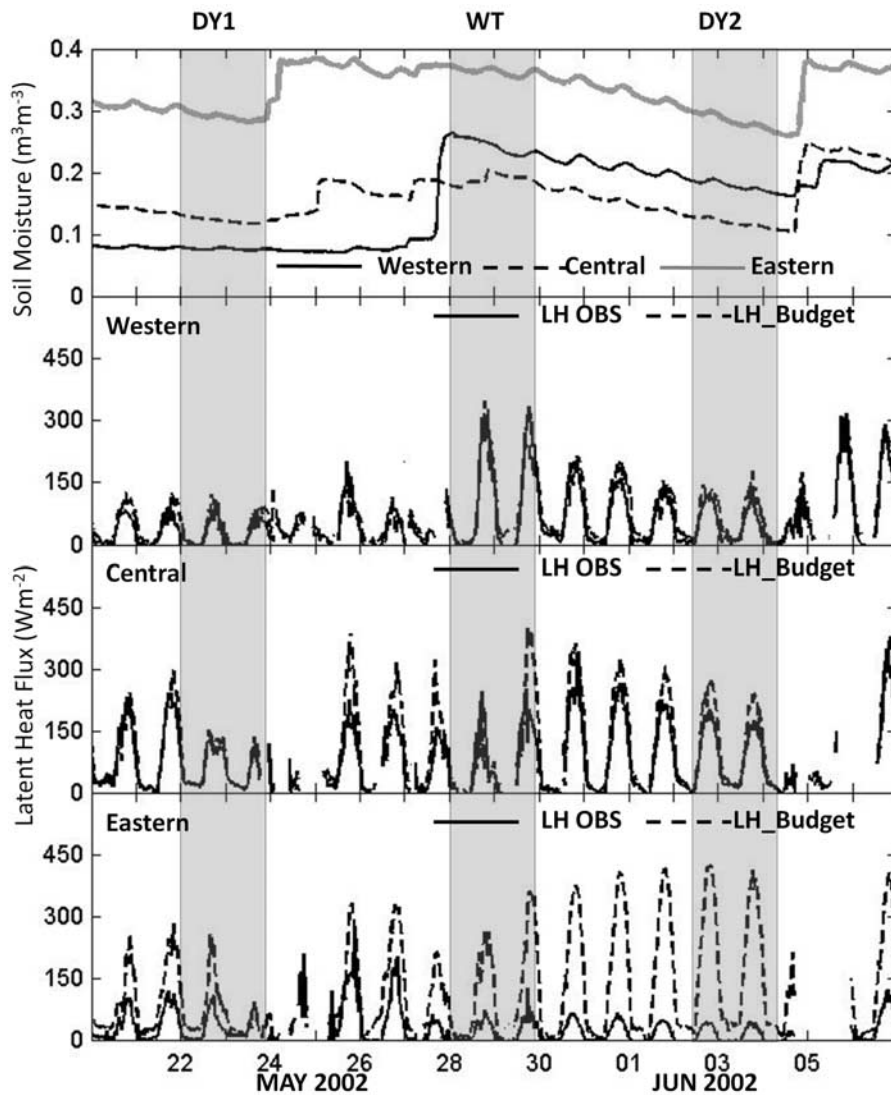

Figure 2. Soil moisture and latent heat flux observations from the ISFF stations during IHOP_2002 and the model time configuration scheme (DY1, from 22 May 0000 UT to 24 May 0000 UT; WT, from 28 May 0000 UT to 30 May 0000 UT; DY2, from 2 Jun 1200 UT to 4 Jun 1200 UT 2002); each line represents a temporal trend of the each ISFF track through average of every three stations.

radiometric, and flux data, which include incident longwave and shortwave radiations, rainfall, sensible heat (SH) flux, LH, ground heat (GH) flux, surface temperature (TS), and soil moisture. These data can be obtained from the Web site: http://www.rap.ucar.edu/research/land/observations/ihop.

[8] The field observations showed some defects during the latent heat flux computation, which is caused by water infiltration problems of several krypton hygrometer (KH2O) sensors [*Chen et al.*, 2007] and by the radio frequency transmission of the station data. Chen et al. stated that those errors were negligible or later reasonably fixed during IHOP_2002. However, large differences between measured LH and the one derived from radiation budget are observed in the ISFF stations around the eastern track up to 400 Wm^{-2} (Figure 2). As shown by prior studies [*Twine et al.*, 2000; *Yates et al.*, 2001], the eddy correlation method used for the LH measurements tends to compute less LH than the one derived from radiation budget. The net radiation (nR) is equal to the sum of LH, GH, and SH. Even though *Chen et al.* [2007] pointed out that this low LH is due to a lack of the consideration of the heat storage in the canopy and energy associated with photosynthesis, the 400 Wm^{-2} is a very large difference. *LeMone et al.* [2007] had excluded the LH observation data in that region and used the one derived from the radiation budget instead. Thus, using the same radiation budget method, we also used LH calculated from nR, SH, and GH in this study, naming it "LH_budget."

2.2. Model Description and Configurations

[9] *Chen and Dudhia* [2001] designed a model coupling technique, using the fifth generation Mesoscale Model (MM5) and the Oregon State University land surface model (OSULSM, or later, Noah LSM), which was used for the WRF model. As the next generation regional-scale forecasting model succeeding MM5 technology and model coupled system, the WRF model is a mesoscale model for numerical weather forecasting and a data assimilation system [*Skamarock et al.*, 2005]. Maintained and supported as a community model to facilitate wide use for research and teaching in the university community, it is suitable for use in a broad spectrum of applications across scales ranging from meters to thousands of kilometers. This includes research and operational numerical weather prediction, data assimilation, parameterized physics research, downscaling climate simulations, driving air quality models, etc., and offers numerous physics options such as microphysics, surface physics, atmospheric radiation physics, and planetary boundary layer physics.

[10] The Noah LSM used for this model coupling approach was originally developed by *Pan and Mahrt* [1987]. Its hydrological physics is based on the diurnally dependent Penman potential evaporation approach [*Mahrt and Ek*, 1984], the multilayer soil model [*Mahrt and Pan*, 1984], and the primitive canopy model [*Pan and Mahrt*, 1987]. This model has been extended with a canopy resistance formulation and a surface runoff scheme by *Chen et al.* [1996] and implemented into the MM5 and WRF model for the model coupling system. In the Noah LSM of the coupled model, ET is expressed as the sum of direct evaporation from the ground and canopy surfaces and transpiration through vegetation [*Chen and Dudhia*,

2001]. Direct ground evaporation (EDIR) is estimated from a simple linear method [*Betts et al.*, 1997], and canopy surface evaporation (EC) is calculated from similar methods by *Noilhan and Planton* [1989] and *Jacquemin and Noilhan* [1990]. Vegetation transpiration (ETT) is very similar to the EC formulation, but canopy resistance is included in its calculation. The canopy resistance, which has been extended by *Chen et al.* [1996] in the Noah LSM, is estimated by the formulation of *Jacquemin and Noilhan* [1990], representing the effects of solar radiation, vapor pressure deficit, air temperature, and soil moisture. The main procedure of the estimation process of surface moisture flux in the Noah LSM is as follows: Once the initial land states, surface characteristics, and atmospheric forcing data are obtained, the model calculates land-atmospheric heat and moisture exchange coefficients with soil conductivity and diffusivity. Then, these coefficients are used to estimate potential evaporation, which becomes the basis of the moisture flux estimation after it is combined with the canopy resistance.

[11] The domain configuration was set up to cover all NCAR ISFF stations with a resolution of 1 km (Figure 1). We set three one-way nesting domains with a 5:1 spatial ratio. From the set of the subject domain (domain 3) over the IHOP_2002 area with 1 km resolution, an outer domain (domain 2) was set with 5 km, and then the mother domain (domain 1) was set to cover nearly half of North America with 25 km resolution. Such domain configuration is controlled by a domain nesting system that allows us to increase the model spatial resolution by the mesh refinement method [*Michalakes*, 2000]. Through this domain nest setting, smaller domains with higher resolutions take and/or give information about boundary conditions from bigger domains with lower resolutions. The area covered by each domain comprises 75 × 55, 206 × 106, and 526 × 186 grid boxes for domain 1, 2, and 3, respectively. Each grid box represents a square area with the given length from the resolutions (25 × 25, 5 × 5, and 1 × 1 km, respectively).

[12] On the basis of the soil moisture time variation observed by the field measurements, we made three simulation sets with separate time periods that represent the temporal heterogeneity of the surface moisture status (Figure 2). According to the ISFF observations, each station showed relatively dry surface conditions until a rainfall event between 24 May and 27 May 2002, and then the relatively moist surface condition gradually decreased from 28 May until the next rainfall event around 4 June 2002. We defined the high moisture period of the surface between the 28 May and 30 May as wet (WT) period, and the dry (DY) period before WT as DY1. The dry period that occurred after WT was labeled DY2. With this time configuration, we expected the sensitivity of the model to respond to the variation of the surface moisture condition when the surface varies from dry to wet or vice versa. We set the model spin-up time for each period with 48 h: From 22 May at 0000 UT to 24 May at 0000 UT for Dry1, from 28 May at 0000 UT to 30 May at 0000 UT for Wet, and from 2 June at 1200 UT to 4 June at 1200 UT for Dry2.

2.3. Parameterization of Vegetation Fraction

[13] There are two popular methods for deriving Fg. One is used in the current coupled WRF/Noah model and

Table 1. Minimum/Maximum NDVI Values for IGBP Land Cover Classification and USGS Land Cover Classification[a]

	IGBP Land Cover Type	USGS Land Cover Type	MODIS
$NDVI_{max}$	Bare and shrubland	Shurbland Mixed shrubland/grassland	0.87
	Grassland	Grassland	0.67
	Cropland	Dryland cropland and pasture Irrigated cropland and pasture	0.86
	Cropland/national vegetation mosaic	Cropland/grassland mosaic Cropland/woodland mosaic	0.86
	Evergreen/deciduous needleleaf forest	Evergreen/deciduous needleleaf forest	0.89
	Deciduous broadleaf forest	Deciduous broadleaf forest	0.89
	Evergreen broadleaf forest	Evergreen broadleaf forest	0.85
	Mixed forest	Mixed forest	0.89
	Savanna	Savanna	0.80
$NDVI_{min}$	All land cover types		0.07

[a]IGBP land cover classification is as in the work of *Montandon and Small* [2008]; USGS land cover classification is as in the model parameter. NDVI, Normalized Difference Vegetation Indices; IGBP, International Geosphere-Biosphere Programme.

derived by the following linear method [*Gutman and Ignatov*, 1998]:

$$Fg = \frac{NDVI - NDVI_{min}}{NDVI_{max} - NDVI_{min}}, \qquad (1)$$

where $NDVI_{min}$ is minimum NDVI (or bare soil NDVI) and $NDVI_{max}$ is maximum NDVI (or full canopy NDVI). The current model uses 0.04 for $NDVI_{min}$ and 0.54 for $NDVI_{max}$, which have been selected as seasonally and geographically invariant constants [*Gutman and Ignatov*, 1998]. The monthly Fg data using a global 5-year AVHRR NDVI (1986 to 1991) have been applied to the model Fg parameter. The other popular method to compute Fg is the quadric model [*Carlson and Ripley*, 1997]:

$$Fg = \left(\frac{NDVI - NDVI_{min}}{NDVI_{max} - NDVI_{min}} \right)^2. \qquad (2)$$

Montandon and Small [2008] pointed out that underestimation of $NDVI_{min}$ causes overestimation of Fg, especially in sparse vegetation areas such as grassland in the western area. This overestimation is minimized when using the quadric Fg method.

[14] Considering the relatively high spatial and temporal resolution for new Fg parameters, we produced Fg from the MODIS data as mentioned above. There are two different MODIS platforms: Terra and Aqua, but we only used data from Terra MODIS owing to data availability in 2002. NDVIs were derived from an 8-day 500 m surface reflectance from MODIS (MOD09A1.4) via http://lpdaac.usgs. gov, using the MODIS sensor band 1 (620–670 nm) and band 2 (841–876 nm) data. Even though MODIS provides daily surface reflectance, which may be able to offer vegetation variation on a daily basis, the data are not viable for this study owing to data loss caused by cloud effects. The selection of 8-day MODIS data was due to the high

temporal resolution used in this study. The MODIS data sets were spatially resized from 500 m to 1 km, 5 km, and 25 km resolutions through data aggregation for domains 1, 2, and 3, respectively. Then, on the basis of the quality information of the MODIS data, bad data pixels, contaminated by cloud effects, were eliminated and replaced to a null value. The applied MODIS data sets to the Fg parameterizations are 8-day, 17 May 2002 data granules for DY1 and 8-day, 25 May 2002 data granules for WT and DY2.

[15] For the determination of $NDVI_{min}$ and $NDVI_{max}$, we used two different methods. One is to select them as invariant constant values among the local MODIS NDVIs in our study area (domain 3). In our case, the selected NDVI values were 0.04 and 0.80 for $NDVI_{min}$ and $NDVI_{max}$, respectively. The other method used in this study is to use a constant $NDVI_{min}$ but variant $NDVI_{max}$. In the physics of canopy resistance applied to the Noah LSM, vegetation parameters such as maximum/minimum stomatal resistance, leaf area index, and leaf cuticular resistance have constant values for each land cover type. Thus, it is likely to be more beneficial to obtain better LH simulation if the Fg derivation is associated with land cover types. In this study, we adopted a constant $NDVI_{min}$ (0.07) and variant $NDVI_{max}$, which were derived using the *Zeng et al.* [2000] method for the 2003 MODIS NDVI data (Table 1). Table 2 summarizes the methods used for the Fg parameterizations in this study. We labeled each method, Base (BS), VEG1, and VEG2, as shown in Table 2.

2.4. HRLDAS Soil Moisture Data Initialization

[16] In order to provide improved land-state initialization for the coupled WRF/Noah model, HRLDAS is being developed at NCAR and executed in the uncoupled mode of the Noah LSM by interpolating land surface variables from observed atmospheric forcing conditions [*Chen et al.*, 2007]. An advantage of HRLDAS is the consistency with the coupled WRF/Noah model system because it uses the same WRF nested grid configurations such as resolution,

Table 2. Summary of Fg Parameters Used in This Study

	Data Source	Input Resolution	Fg Model
BS[a]	5-year AVHRR NDVI (1986–1991)	Monthly 0.15°	Linear [$NDVI_{min}$: 0.04 $NDVI_{max}$: 0.54]
VEG1	2002 MODIS surface reflectance	8 day 1 km	Linear [$NDVI_{min}$: 0.04 $NDVI_{max}$: 0.8 (from local values)]
VEG2	2002 MODIS surface reflectance	8 day 1 km	Quadric [$NDVI_{min}$: 0.07 $NDVI_{max}$: variant (Table 1)]

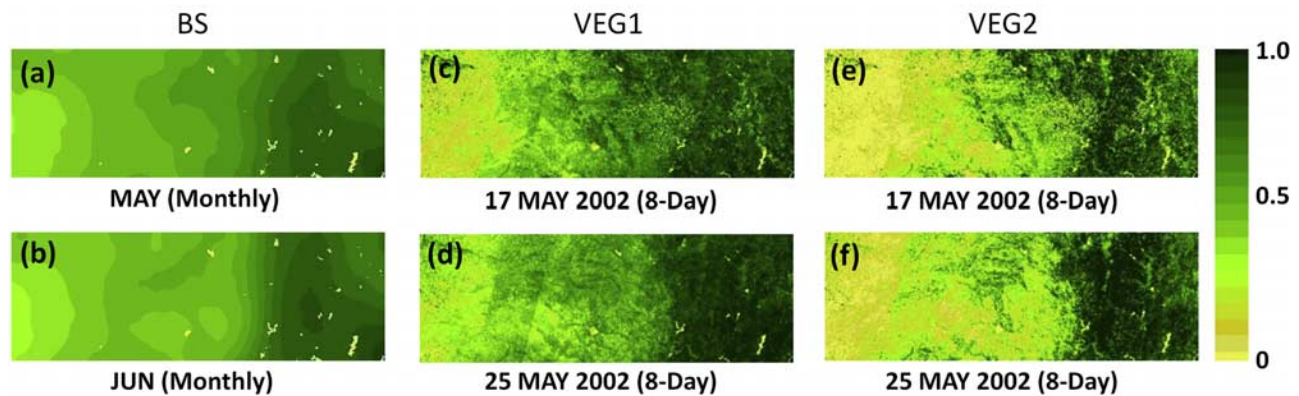[a]The method originally used for the WRF model Fg parameter.

Figure 3. Fg images for BS, VEG1, and VEG2 cases in 1 km spatial resolution: (a) DY1 and WT of the BS case, (b) DY2 of the BS case, (c and e) DY1 of the VEG1 and VEG2 cases, respectively, and (d and f) for WT and DY2, respectively, of the VEG1 and VEG2 cases.

grid points, and projection, and the same land surface parameters such as land use, soil texture, terrain height, and vegetation properties. HRLDAS reads those sources from WRF input files generated by WRF Standard Initialization (SI) or the WRF Preprocessing System (WPS). Atmospheric forcing data used on HRLDAS includes hourly 4 km NCEP stage IV rainfall analyses data [*Fulton et al.*, 1998], hourly 0.5 degree downward solar radiation derived from the Geostationary Operational Environmental Satellite (GOES) [*Pinker et al.*, 2003], and three hourly atmospheric analyses from NCEP Eta Data Assimilation System (EDAS) [*Rogers et al.*, 1995]. With the model basis of Noah LSM, HRLDAS uses four soil layers to present daily, weekly, and seasonal soil moisture variation.

[17] In this study, we produced input files for HRLDAS using WRF SI. *Chen et al.* [2007] experimented on HRLDAS spin-up dependency to find out its equilibrium state for various soil layers and pointed out that fine soil texture with low hydraulic conductivity requires longer spin-up time to reach the equilibrium state. On the basis of their study, we ran HRLDAS for about 13 months, which is a typical runtime for most soil types, starting from April 2001. The soil moisture generated by HRLDAS was used for the model initial conditions, combined with the quadric Fg model parameterization method.

3. Results

3.1. Vegetation Effect From the Fg Parameterizations

[18] Figure 3 shows Fg images of the study area derived from the methods discussed in section 2.3. As expected, the Fg in the BS case does not properly represent the spatial distribution of vegetation for the 1 km resolution. On the other hand, Fg derived from MODIS data seem to have much more detailed information about the vegetation spatial variability. Differences in contrast of the Fg distribution from west to east is observed in between the VEG1 and VEG2 cases. The Fg shows the west–east spatial distribution from about 0.35 to 0.75 in the BS case, about from 0.15 to 0.85 in the VEG1 case, and about 0.05 from 0.9 to in the VEG2 case. After the Fg parameterization, the Fg values in the western ISFF station sties (0.2 in VEG1 and 0.09 in VEG2 on average) were lower than the BS case (0.37 on

average) while those in the eastern region were raised (0.71 in BS, 0.78 in VEG1, and 0.79 in VEG2 on average).

[19] Figure 4 shows the temporal variations of simulated land surface variables and Table 3 provides their statistical comparisons to the ISFF observations with correlation coefficients (R square values from regression analyses) and Root Mean Square Errors (RMSE). Relatively low correlations were observed in GH and LH in the eastern area while the other areas showed good correlation with the observations.

[20] As mentioned above, in order to test only the vegetation effect by Fg parameterization, the nine-point soil moisture initialization was conducted simply by replacing the soil moisture values of the nine-point grid cells in model initial inputs. The target domain configured in the model has 1 km × 1 km spatial resolution, and heterogeneity in spatial distribution, for instance, of soil moisture and vegetation is often observed in such a small area unit or even smaller ones. With this data replacement for the soil moisture initial condition, low atmospheric variation in each simulation period resulted in reasonable soil moisture simulations in the coupled WRF/Noah model. It should be noted that there was no observation of any substantial rainfall during each period, except from 5 to 20 mm of precipitation at the end of DY1. After the soil moisture initialization, the soil moisture initial conditions were lowered in the western and central areas and raised in the eastern area from the original ETA model data.

[21] The effects of the Fg parameter on TS simulation were observed mainly during DY2 in the eastern area, showing about a 5 K decrease of the diurnal peaks, while those of the other regions showed slight or no improvement. RMSE of TS simulations, however, did not show any significant difference among the cases. The average RMSE of TS simulations were about 3 K. The TS underestimation in the eastern area is mostly found in locations where soil moisture was around $0.38 \text{ m}^3 \text{ m}^{-3}$. This does not indicate the soil moisture effect from the data replacement, but rather the vegetation effect from the Fg parameterizations. Increase in the Fg parameter caused lower TS. This is also supported by the HRLDAS test as described in section 3.2.
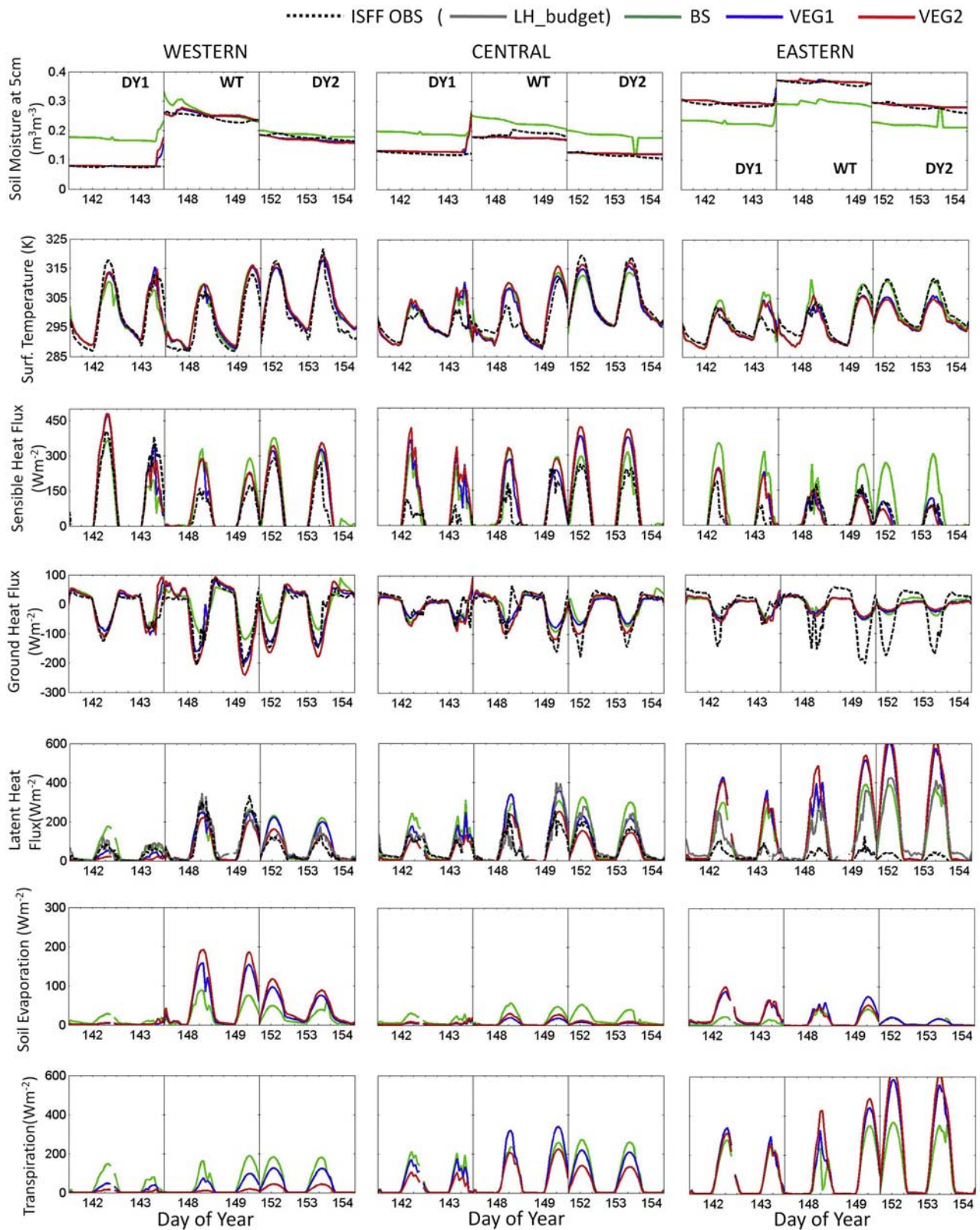
Figure 4. Temporal variations of land surface variables simulated by the WRF/Noah model and their comparisons to the ISFF observations for the BS, VEG1, and VEG2 cases. Each point was averaged for the three ISFF sites in each track.

Table 3. Correlation Coefficients and RMSE of Simulated Land Surface Variables to ISFF Observations[a]

		Western		Central		Eastern	
	Case	R^2	RMSE	R^2	RMSE	R^2	RMSE
TS (K)	BS	0.86	3.71	0.78	3.57	0.82	2.91
	VEG1	0.92	3.09	0.81	3.41	0.82	2.98
	VEG2	0.91	3.47	0.79	3.95	0.78	3.30
SH (Wm^{-2})	BS	0.67	78.28	0.68	76.35	0.62	91.07
	VEG1	0.81	62.60	0.75	85.90	0.73	38.33
	VEG2	0.78	70.16	0.73	106.55	0.69	40.74
GH (Wm^{-2})	BS	0.80	36.56	0.60	33.37	0.66	51.25
	VEG1	0.89	24.23	0.72	30.02	0.62	52.03
	VEG2	0.89	33.53	0.74	27.38	0.50	54.09
LH (Wm^{-2})	BS	0.72	47.51	0.81	69.57	0.58	151.52
	VEG1	0.76	39.66	0.80	58.57	0.56	218.63
	VEG2	0.83	33.14	0.75	37.03	0.53	234.86
LH_Budget (Wm^{-2})	BS	0.74	46.70	0.73	63.67	0.81	61.94
	VEG1	0.79	40.72	0.70	59.03	0.87	100.80
	VEG2	0.83	38.05	0.66	57.92	0.87	114.43

[a]RMSE, Root Mean Square Errors; ISFF, Integrated Surface Flux Facilities.

[22] While TS underestimations were observed, SH simulations showed significant improvement during WT and DY2 in the eastern area. The SH simulations agree very closely with the observations with about a 200 Wm^{-2} decrease during DY2 in that region. RMSE of the SH also supports this improvement, which was observed in both of the Fg parameterizations. In the eastern area, the RMSE of SH improved from about 90 Wm^{-2} to 40 Wm^{-2}. SH values of the diurnal peaks in that region decreased by 100 Wm^{-2} during DY1, 120 Wm^{-2} during WT, and 200 Wm^{-2} during DY2, which are very close values to the SH observations. No substantial difference was observed between VEG1 and VEG2 because the Fg parameters were very similar in the eastern stations. On the other hand, SH during DY2 in the central track showed overestimations and increased by 100 Wm^{-2} from that of the BS case. RMSEs also increased by 30 Wm^{-2} in the VEG2 case. The other periods (DY1 and WT) in the central area showed no significant changes in SH simulations. Meanwhile, in the western area, the new Fg parameters were less influential and SH overestimation during DY1 of the VEG1 and VEG2 cases was interpreted as having a high sensitivity of the model to soil moisture variation in that region. This will be discussed further in section 3.2.

[23] The simulated GH flux did not show any vegetation effect in the highly vegetated areas. The low diurnal variations of the simulated GH in the eastern area were not improved either by the Fg parameterizations or soil moisture initialization. GH RMSEs in this region showed over 50 Wm^{-2}, which is larger by about 20 Wm^{-2} compared with the other regions. Considering the range of the GH diurnal cycle (from about 80 Wm^{-2} to 200 Wm^{-2}), this error is quite significant. The greatest difference between the observations and the simulations were up to 150 Wm^{-2}. On the other hand, some simulation improvements especially in the VEG1 case were observed during WT and DY2 in the region with less vegetation (the western area).

[24] LH simulations were very sensitive to Fg in highly vegetated areas. Table 3 shows good correlations with the observations (the LH_budget case) in that area. Apart from

the LH measurement error mentioned in the section 2.1, noticeable LH overestimations in that area were observed and the differences from the LH_budget observation was as much as 200 Wm^{-2}. This LH overestimation has also been reported in previous studies [*Chen et al.*, 2007; Hong et al., submitted manuscript, 2009] in which the studies used the Noah LSM implemented into HRLDAS and into the WRF model, respectively. Any substantial difference between the VEG1 and VEG2 cases was not observed in the eastern region, but the central (in all periods) and western areas (during DY2) show improved simulations in the VEG2 case. The error statistics through RMSEs of the LH also demonstrates this LH overestimation results. RMSE were observed to be better in the VEG1 (about 6 Wm^{-2} and 3.5 Wm^{-2} improvements in the western and central area, respectively) and VEG2 (about 7.5 Wm^{-2} and 6 Wm^{-2} improvements in the western and central area, respectively) cases in relatively low vegetated areas but worse in the eastern area (about 39 Wm^{-2} and 52 Wm^{-2} worsened in VEG1 and VEG2 cases, respectively) as verified with LH_budget observations. When compared with LH observations, the central area shows better results with a lower RMSE (about 39 Wm^{-2} improvements in the VEG2 case). The analyses of the temporal variations of the ET components, EDIR (direct evaporation from bare ground) and ETT (vegetation transpiration), were performed in order to understand the LH overestimations in the eastern area. EC generally occurs in a very short time, taking a very small portion of the total ET after precipitation. As seen from section 2.2, the model was configured to avoid any precipitation during the spin-up periods. It should be noted that we omitted analyzing EC in this result section. EC was a very small portion of our model simulations (less than 10 Wm^{-2} in average) and can be ignored for LH analyses. According to the result, the LH overestimation is mainly due to the overestimation of vegetation transpiration. LHs were overestimated in both VEG1 and VEG2 cases with about 250 Wm^{-2} more than those of the BS case. Even though BS is not a good reference for transpiration analyses, the case studies provide enough results to interpret model responses to vegetation parameters. With the HRLDAS case study, we present that the vegetation effect is more responsible for the LH overestimation than soil moisture variation. This issue will be discussed further in section 3.2.

3.2. Soil Moisture Effect From HRLDAS Initialization

[25] Figure 5 shows the soil moisture comparison between that derived from Eta and HRLDAS. As shown in section 3.1, the soil moisture in the BS case shows much less information about spatial variability than the one from HRLDAS, and the soil moisture spatial contrast from east to west is also obvious. The very low soil moisture area in the west (areas with very red color) corresponds to a sandy soil surface that generally has high hydraulic conductivity. As mentioned in section 2.4, the soil moisture initialization test of HRLDAS was performed in combination with the Fg parameterization (the quadric method).

[26] Figure 6 shows the temporal variation of the surface variables simulated by the coupled WRF/Noah model and Table 4 provides the statistical analyses of these data. Relatively good correlations with observations were observed for most variables except GH and LH in the eastern
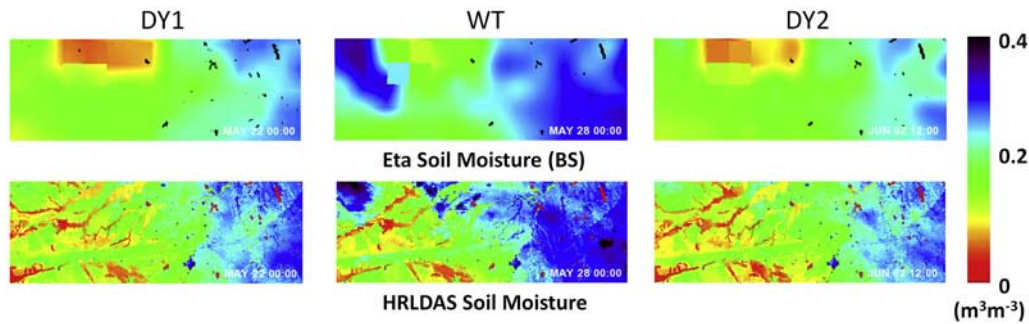
Figure 5. Soil moisture images of the model input, interpolated for 1 km spatial resolution from (top) Eta model and (bottom) HLRDAS.

area, which is similar to the Fg cases. The low coefficient of LH simulations was improved when it was compared to the LH_budget (from 0.49 to 0.91). Simulated soil moisture variations by HRLDAS were improved in the western and central regions but showed almost no change in the eastern area. This soil moisture improvement did not show any significant effect on TS simulations in the coupled WRF/ Noah model. The new Fg in the HRLDAS case, however, showed a very similar pattern to the TS diurnal cycle seen in the VEG2 cases. Moreover, the TS underestimations in the eastern area support the Fg effect as discussed in section 3.1. Meanwhile, the second TS peak values in the western area make possible an interesting interpretation about the model. In the soil moisture variations of the VEG2 and HRLDAS cases, HRLDAS showed higher soil moisture ($0.13 \text{ m}^3 \text{ m}^{-3}$) than in VEG2 ($0.08 \text{ m}^3 \text{ m}^{-3}$), but the second TS peak value during DY1 was higher in HRDAS (319 K) than that in VEG2 (315 K). This result of the TS increase in spite of soil moisture increase in lowly vegetated areas indicates a greater sensitivity of the model to the Fg parameter but not to soil moisture (Fg was 0.09 in the western station sites of VEG2 in average).

[27] Unlike the improved SH simulations in the VEG1 and VEG2 cases for the eastern track, the ones of the HRLDAS case did not closely approach the observed diurnal cycle because soil moisture did not change in that region after the HRLDAS soil moisture initialization. This indicates that the SH simulation is affected not only by vegetation but also by soil moisture variation. While the central area showed similar results as in the VEG2 case, the western area indicated the model sensitivity to soil moisture variation as discussed in section 3.1. During the WT period in the western area, soil moisture did not display any quantifiable variability in all cases in this study. This resulted in little change of SH simulations in that period, indicating low sensitivity to the Fg parameter. On the other hand, while soil moisture was lowered to $0.1 \text{ m}^3 \text{ m}^{-3}$ during DY1 in that region, the SH of the VEG2 case increased by about 100 Wm^{-2} in the first peak time of that period. A similar result was observed in the HRLDAS case (SH increased by 50 Wm^{-2}), but the difference in the SH peak values between these two cases explains that the SH overestimation is caused by soil moisture variation in lowly vegetated areas. GH in the coupled model is not sensitive to soil moisture variation and demonstrate similar results to the VEG1 and VEG2 cases.

[28] LH overestimations from ETT overestimation were also observed in the eastern area in the HRLDAS case, indicating the new Fg effects on the model sensitivity. From the HRLDAS case study, however, we found that the soil moisture variation was also influential on the ETT overestimation. Given that there was no soil moisture change in the HRLDAS case, the ETT showed less overestimation (up to 550 Wm^{-2}) than that found in the VEG1 or VEG2 cases (up to 630 Wm^{-2}). Thus, the ETT difference between the HRLDAS and the VEG1 or VEG2 cases implies the effect of soil moisture variation on the model sensitivity. In the western area, both effects of vegetation and soil moisture on ETT simulations were observed. When Fg and soil moisture decreased during DY1, ETT also decreased. EDIR simulations also support the dual effects as demonstrated during the WT period in the western area. EDIR increased more (up to about 200 Wm^{-2}) owing to the effect of the Fg parameter alone than it did when the effects of the Fg parameter and soil moisture decrease (up to about 160 Wm^{-2}) were combined. The RMSE of the LH simulations in the HRLDAS case showed significant improvement in the central area more than other cases. Meanwhile, the LH simulations seem to demonstrate better results in the eastern area for the VEG1 or VEG2 cases (from the statistics with the LH_budget), but this did not lead to any improvement from the BS case (Table 3).

4. Conclusion and Discussion

[29] In this study, we tested model sensitivity to vegetation and soil moisture variation to evaluate the model's improvement due to Fg parameterization and HRLDAS soil moisture initialization. The two Fg parameterization methods, the linear and quadric methods (VEG1 and VEG2, respectively) with more recent satellite-observed NDVI from MODIS, were used and they resulted in better spatial west–east contrast of Fg distribution, comparing that in the BS case which uses the linear method with old NDVI from AVHRR (i.e., less vegetation in west and higher vegetation in east). We demonstrated vegetation effects on the coupled model simulations by the Fg parameterization in either a positive or negative way in terms of the model improvement. We obtained underestimation of TS, overestimation of LH, and improvements in SH in the highly vegetated region (the eastern area) and underestimation of GH in the lowly vegetated region (the western area) for VEG1 and VEG2 cases. According to the statistical analyses,
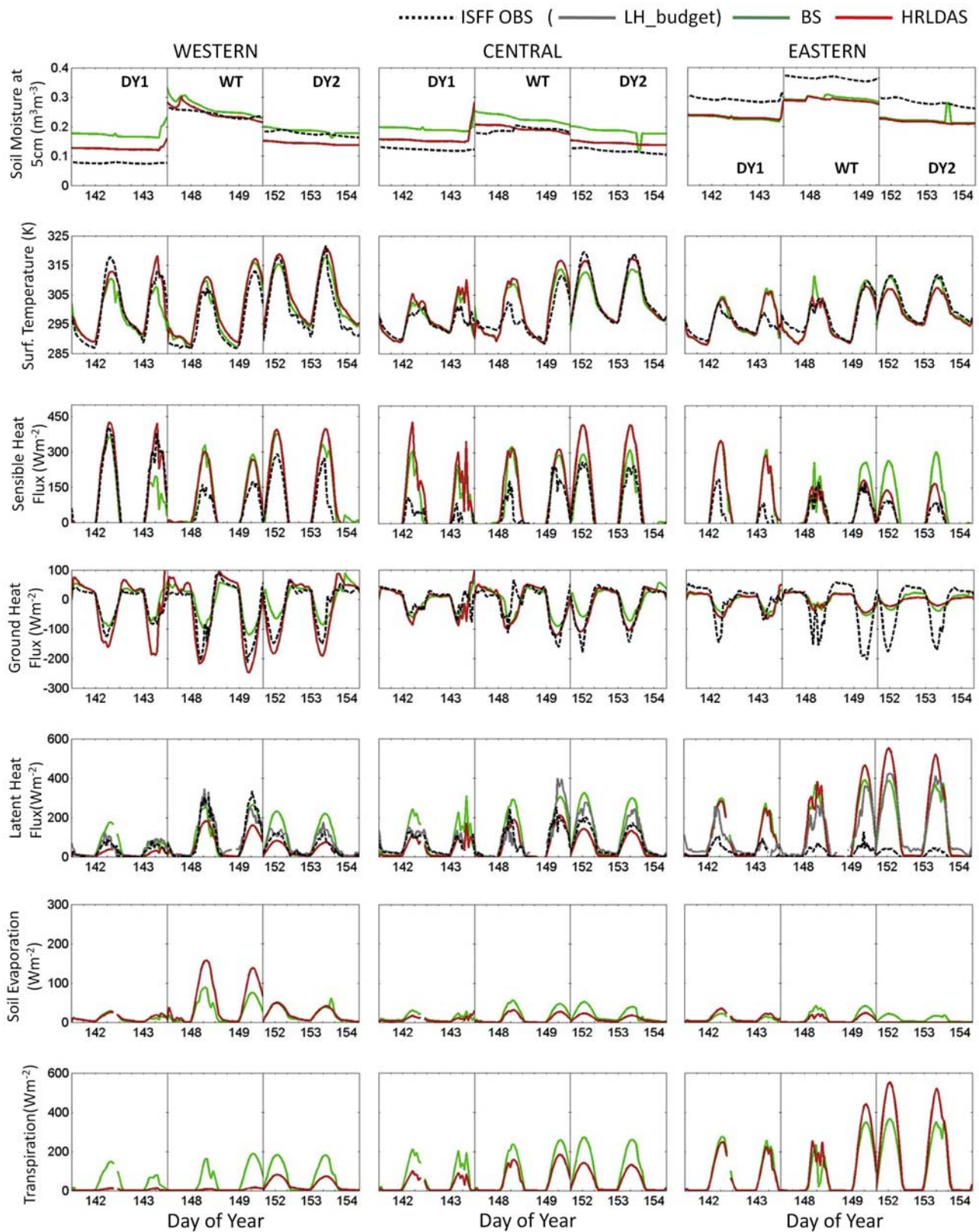
Figure 6. Temporal variations of land surface variables simulated by the WRF/Noah model and their comparisons to the ISFF observations for the BS and HRLDAS and VEG2 cases. Each point was averaged for the three ISFF sites in each track.

Table 4. Correlation Coefficients and RMSE of Simulated Land Surface Variables to ISFF Observations for the HRLDAS Case[a]

	Western		Central		Eastern	
	R^2	RMSE	R^2	RMSE	R^2	RMSE
TS(K)	0.92	3.83	0.80	4.01	0.79	2.90
SH(Wm^{-2})	0.86	68.53	0.80	102.86	0.67	63.85
GH(Wm^{-2})	0.89	42.72	0.73	28.39	0.50	54.47
LH(Wm^{-2})	0.94	39.64	0.77	34.99	0.49	188.61
LH_Budget	0.90	44.91	0.70	60.53	0.91	69.46

[a]HRLDAS, High-Resolution Land Data Assimilation System.

we obtained improved results in SH simulations in the eastern area and in LH simulations in the western and central areas for both the VEG1 and VEG2 cases. Meanwhile, the HRLDAS case, combined with the VEG2 method, indicates both effects of vegetation and soil moisture variation. There was some improvement from the inclusion of the HRLDAS soil moisture initialization, but this needs to be validated through further research with a longer period of simulation.

[30] Among the various changes after the Fg parameterizations and/or HRLDAS soil moisture initialization, noticeable results were found including the low GH variability and LH overestimation in the eastern stations. According to the physics of the Noah LSM, soil temperature plays a key role in GH estimations and soil temperature is a function of soil moisture [Chen et al., 2003]. Thus, for the VEG1 or VEG2 cases in the western area, lowered GH peak values during WT and DY2 are due to soil temperature increases induced by the Fg decrease from the newer Fg parameterizations. Accordingly, the fact that a large Fg value in the eastern area (over 0.7 in all study cases) resulted in very low GH variability implies low soil temperature in that region possibly due to the canopy shadow effect. With both results, this study indicates a high sensitivity of GH simulation to the Fg parameter. Nonetheless, the low GH variability from the model in the eastern area is still problematic when compared to GH observations. This may imply an excessive effect due to vegetation.

[31] On the other hand, LH simulations in the eastern area were also very sensitive to vegetation, showing an overestimation of ETT. Finding the answer for the LH overestimation is quite challenging. There may be many causes for LH overestimations and we examined some possibilities as follows: (1) initial soil moisture changes and (2) overestimation of wind velocity. The first case has been proved to not be very effective through this study. High wind intensity will be consequently followed by high ETT, but we did not observe any overestimation of wind from the model in the eastern area (Figure 7). Even though the wind velocity of the east–west component during DY2 in that area increased after the Fg parameterizations, a lower variation from the model was observed compared to the wind observations (Figure 7). However, we present that the cause of this problem in the model may be related to that of the low variability of GH simulations. We calculated the nR from simulated LH, GH, and SH using the radiation budget method (Figure 8) and found an interesting fact about the model. There is a good match with the R observations during DY2 in the eastern area. This match of R in spite of the low reliability of LH and GH simulations is due to a counterbalancing of the two parameters. Further research is

warranted to understand the R analyses through the investigations of simulated longwave and shortwave radiations. R from the radiation budget may imply a connection between LH and GH related to the vegetation effect. For instance, LH may be improved when the model can be improved in GH simulations related to vegetation. Other possible answers about the ETT overestimations may be found in the relation with plant water stress and surrounding air conditions such as CO_2 levels, which affect the leaf stomata opening and closing and are the major factor in the control of vegetation transpiration [Betts et al., 1997; Hong et al., 2007].

[32] Describing horizontal portion of vegetation on a given surface area, Fg in the NOAH LSM has been played a key role as a determinant coefficient in partitioning ET into soil evaporation and vegetation transpiration [Jacquemin and Noilhan, 1990; Chen and Dudhia, 2001]. For example, increase Fg in a certain surface area results in increase of transpiration and decrease of soil evaporation under the same surface moisture condition. However, Fg is not involved just in LH estimation in the model but also all surface energy balance comprehensively. For example, under controlled precipitation condition in this model, although surface soil moisture variations were same in the eastern area of BS and HRLDAS cases, the model shows significant difference in total LH amount between them especially in the DY period. Of course, there are other important parameters representing vegetation properties. Most of all, land use and land cover (LULC) data are very important because each land cover type defines other properties of vegetated surface such as surface albedo, roughness length, and etc. Thus, for the compatibility of
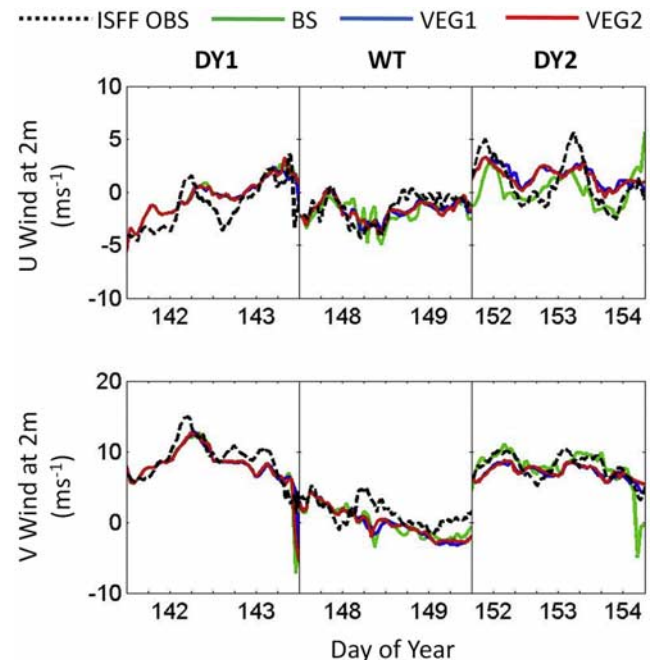

Figure 7. Temporal variations of (top) east–west (U) component and (bottom) north–south (V) component wind velocity simulations and their comparison to the ISFF observations for the BS, VEG1, and VEG2 cases in the eastern track.
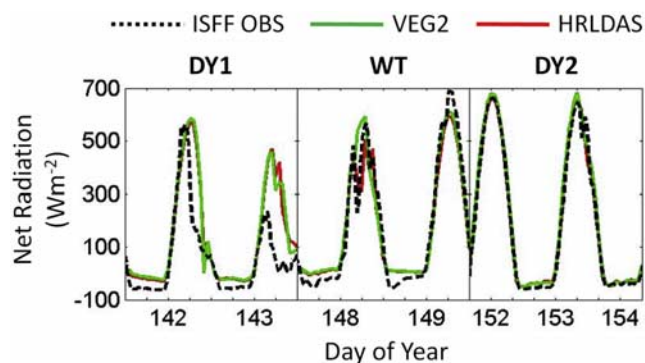
Figure 8. Temporal variations of net radiation calculated from LH, GH, and SH simulations and their comparison to the ISFF observations for the VEG2 and HRLDAS cases in the eastern track.

land cover data usage, we used very high spatial resolution data for LULC: 30 s in degree which is less than 1 km in the central area of United States. LULC has been obtained from USGS/EROS (via http://edcdaac.usgs.gov/glcc/globe_int. html). Even though the accuracy or reliability of LULC used in this study may be another issue for its contribution to model accuracy, but considering the temporal variation of LULC is much lower than that of vegetation fraction, its effect to surface variation is little in such a small time span in this study. In addition, the effects of interactions among neighboring grid areas within the domains due to nine-point soil moisture initialization cannot be ignored, but they have been considered not to be contrary to the conclusion or rather supportive. If the effects were substantial, the model sensitivity to such soil moisture changes might be diminished. The model rather showed that soil moisture changes were less effective than change of vegetation in the comparison between BS and HRLDAS cases.

[33] It is difficult to conclude what experiment performed in the coupled model system resulted in better or improved estimations than any others with this study, but instead, this study indicates that the model sensitivities are not reliable with improved vegetation parameters. There may be limited interpretations about the model sensitivity to soil moisture because of the lack of its observation in this study. While considering recent technology about remote sensing has been monitoring global and continuing vegetation changes of the earth surface with very high spatial and temporal resolution such as NDVI, the model sensitivity to vegetation fraction will need to be diversely tested in more extended area and in longer time span. Moreover, if the studies are combined with more varied remote sensing data such as soil moisture observations by the Advanced Microwave Scanning Radiometer (AMSR), the development of numerical weather forecasting models will be enhanced.

References

Betts, R. A., P. M. Cox, S. E. Lee, and F. I. Woodward (1997), Contrasting physiological and structural vegetation feedbacks in climate change simulations, *Nature*, *387*, 796–799, doi:10.1038/42924.

Carlson, T. N., and D. A. Ripley (1997), On the relation between NDVI, fractional vegetation cover, and leaf area index, *Remote Sens. Environ.*, *62*, 241–252, doi:10.1016/S0034-4257(97)00104-1.

Chen, F., and J. Dudhia (2001), Coupling an advanced land surface-hydrology model with the Penn State-NCAR MM5 modeling system. Part I: Model implementation and sensitivity, *Mon. Weather Rev.*, *129*, 569–585, doi:10.1175/1520-0493(2001)129<0569:CAALSH>2.0.CO;2.

Chen, F., K. Mitchell, J. Schaake, Y. Xue, H. Pan, V. Koren, Q. Y. Duan, M. Ek, and A. Betts (1996), Modeling of land surface evaporation by four schemes and comparison with FIFE observations, *J. Geophys. Res.*, *101*(D3), 7251–7268, doi:10.1029/95JD02165.

Chen, F., Z. Janjic, and K. Mitchell (1997), Impact of atmospheric surface layer parameterization in the new land-surface scheme of the NCEP Mesoscale Eta numerical model, *Boundary Layer Meteorol.*, *85*, 391–421, doi:10.1023/A:1000531001463.

Chen, F., D. N. Yates, H. Nagai, M. LeMone, K. Ikeda, and R. Grossman (2003), Land surface heterogeneity in the Cooperative Atmosphere Surface Exchange Study (CASES-97). Part I: Comparing modeled surface flux maps with surface-flux tower and aircraft measurements, *J. Hydrometeorol.*, *4*, 196–218, doi:10.1175/1525-7541(2003)4<196:LSHITC>2.0.CO;2.

Chen, F., et al. (2007), Description and evaluation of the characteristics of the NCAR High-Resolution Data Assimilation System, *J. Appl. Meteorol. Climatol.*, *46*, 694–713, doi:10.1175/JAM2463.1.

Fulton, R. A., J. P. Breidenbach, D. J. S. Seo, D. A. Miller, and T. O'Bannon (1998), The WSR-88D rainfall algorithm, *Weather Forecast.*, *13*, 377–395, doi:10.1175/1520-0434(1998)013<0377:TWRA>2.0.CO;2.

Gutman, G., and A. Ignatov (1998), The derivation of the green vegetation fraction from NOAA/AVHRR data for use in numerical weather prediction models, *Int. J. Remote Sens.*, *19*(8), 1533–1543, doi:10.1080/014311698215333.

Hong, S., V. Lakshmi, and E. E. Small (2007), Relationship between vegetation biophysical properties and surface temperature using multi-sensor satellite data, *J. Clim.*, *20*, 5593–5606, doi:10.1175/2007JCLI1294.1.

Jacquemin, B., and J. Noilhan (1990), Sensitivity study and validation of a land surface parameterization using the HAPEX-MOBILHY data set, *Boundary Layer Meteorol.*, *52*, 93–134, doi:10.1007/BF00123180.

LeMone, M. A., F. Chen, J. G. Alfieri, M. Tewari, B. Geerts, Q. Miao, R. L. Grossman, and R. L. Coulter (2007), Influence of land cover and soil moisture on the horizontal distribution of sensible and latent heat flux in southeast Kansas during IHOP_2002 and CASES-97, *J. Hydrometeorol.*, *8*, 68–87, doi:10.1175/JHM554.1.

Mahrt, L., and K. Ek (1984), The influence of atmospheric stability on potential evaporation, *J. Appl. Meteorol.*, *23*, 222–234, doi:10.1175/1520-0450(1984)023<0222:TIOASO>2.0.CO;2.

Mahrt, L., and H. L. Pan (1984), A two-layer model of soil hydrology, *Boundary Layer Meteorol.*, *29*, 1–20, doi:10.1007/BF00119116.

Michalakes, J. (2000), A parallel runtime system library for regional atmospheric models with nesting, in *Structured Adaptive Mesh Refinement (SAMR) Grid Methods*, *IMA Volumes Math. Appl.*, vol. 117, pp. 59–74, Springer, New York.

Montandon, L. M., and E. E. Small (2008), The impact of soil reflectance on the quantification of the green vegetation fraction from NDVI, *Remote Sens. Environ.*, *112*, 1835–1845, doi:10.1016/j.rse.2007.09.007.

Noilhan, J., and S. Planton (1989), A simple parameterization of land surface processes for meteorological models, *Mon. Weather Rev.*, *117*, 536–549, doi:10.1175/1520-0493(1989)117<0536:ASPOLS>2.0.CO;2.

Pan, H. L., and L. Mahrt (1987), Interaction between soil hydrology and boundary-layer development, *Boundary Layer Meteorol.*, *38*, 185–202, doi:10.1007/BF00121563.

Pielke, R. A., T. J. Lee, J. H. Copeland, J. L. Eastman, C. L. Ziegler, and C. A. Finley (1997), Use of USGS-provided data to improve weather and climate simulations, *Ecol. Appl.*, *7*(1), 3–21.

Pinker, R. T., et al. (2003), Surface radiation budgets in support of the GEWEX Continental Scale International Project (GCIP) and the GEWEX Americas Prediction Project (GAPP), including the North American Land Data Assimilation System (LDAS) project, *J. Geophys. Res.*, *108*(D22), 8844, doi:10.1029/2002JD003301.

Rogers, E., D. G. Deaven, and G. J. DiMego (1995), The regional analysis system for the operational "early" Eta model: Original 80-km configuration and recent changes, *Weather Forecast.*, *10*, 810–825, doi:10.1175/1520-0434(1995)010<0810:TRASFT>2.0.CO;2.

Skamarock, W. C., J. B. Klemp, J. Dudhia, D. O. Gill, D. M. Barker, W. Wang, and J. D. Powers (2005), A description of the advanced research of WRF version 2, *Tech. rep. TN-468+STR*, Natl. Cent. for Atmos. Res., Boulder, Colo.

Twine, T. E., W. P. Kustas, J. M. Norman, D. R. Cook, P. R. Houser, T. P. Meyers, J. H. Prueger, P. J. Starks, and M. L. Wesely (2000), Correcting eddy-covariance flux underestimates over a grassland, *Agric. For. Meteorol.*, *103*, 279–300, doi:10.1016/S0168-1923(00)00123-4.

Venäläinen, A., T. Salo, and C. Fortelius (2006), The use of numerical weather forecast predictions as source of data for irrigation modeling, *Meteorol. Appl.*, *12*(4), 307–318, doi:10.1017/S135048270500188X.

Weckwerth, T. M., D. B. Parsons, S. E. Koch, J. A. Moore, M. A. Lemone, B. B. Demoz, C. Flamant, B. Geerts, J. Wang, and W. F. Feltz (2004), An overview of the International H_2O Project (IHOP_2002) and some preliminary highlights, *Bull. Am. Meteorol. Soc.*, *85*(2), 253–277, doi:10.1175/BAMS-85-2-253.

Yates, D. N., F. Chen, M. A. LeMone, R. Qualls, S. P. Oncley, R. Grossman, and E. Brandes (2001), A Cooperative Atmosphere-Surface Exchange Study (CASES) data set for analyzing and parameterizing the effects of land surface heterogeneity on area-averaged surface heat fluxes, *J. Appl. Meteorol.*, *40*, 921–937, doi:10.1175/1520-0450(2001)040<0921:ACASES>2.0.CO;2.

Zeng, X., R. E. Dickinson, A. Walker, and M. Shaikh (2000), Derivation and evaluation of global 1-km fractional vegetation cover data for land modeling, *J. Appl. Meteorol.*, *39*, 826–839, doi:10.1175/1520-0450(2000)039<0826:DAEOGK>2.0.CO;2.

Zeng, X., M. Shaikh, Y. Dai, R. E. Dickinson, and R. Myneni (2002), Coupling of the common land model to the NCAR community climate model, *J. Clim.*, *15*, 1832–1854.

———————————

F. Chen, K. W. Manning, and M. Tewari, National Center for Atmospheric Research, Boulder, CO 80307, USA. (feichen@ucar.edu; mukul@ucar.edu; kmanning@ucar.edu)

S. Hong and V. Lakshmi, Department of Geological Sciences, University of South Carolina, Columbia, SC 29201, USA. (shong@geol.sc.edu; venkat-lakshmi@sc.edu)

E. E. Small, Department of Geological Sciences, University of Colorado at Boulder, Boulder, CO 80309, USA. (Eric.Small@colorado.edu)